The Role of Powder Preparation Method in Enhancing Fracture Toughness of Zirconia Ceramics with Low Alumina Amount

I. Danilenko[*], T. Konstantinova, G. Volkova, V. Burkhovetski, V. Glazunova

Donetsk Institute for Physics and Engineering NAS of
Ukraine, 83114, Donetsk, Ukraine, R. Luxemburg str. 72,

Abstract

In most cases zirconia-alumina composites for scientific investigations and industry are prepared by means of mechanical mixing of powders, compaction and sintering. In our opinion, this is one of the reasons for the low values for fracture toughness of the sintered materials. In this study, we investigated the effect of nanopowder synthesis methods on the structure and mechanical properties of 3Y-TZP/alumina ceramic composites and determined the mechanisms involved in composite toughening. We show that the addition of a small amount of alumina (1 – 2 wt%) to zirconia ceramics has the potential to increase the fracture toughness of zirconia ceramics.

The starting powders were obtained by means of co-precipitation and ball milling. It turned out that at equal density, bending strength and hardness values, the fracture toughness in ceramic composites sintered from co-precipitated nanopowders is higher in comparison with fracture toughness values in matrix material and traditional 3Y-TZP/alumina composites. We believed that the role of the crack deflection process in ceramic composites sintered from co-precipitated nanopowders increased significantly. This can be conditioned by means of a series of processes for composite structure formation during precipitation, crystallization, and sintering of nanopowders.

Keywords: 3Y-TZP, fracture toughness, composite, Al_2O_3, structure characterization

I. Introduction

A major limitation to the application of ceramics is their low fracture toughness. Focus studies on ceramic materials are improving their resistance to crack propagation. There are two ways to improve the situation: i) enhancement of the materials structure – transition to nanostructured materials or ii) creation of composite/nanocomposite structures – incorporation of second-phase inclusions that prevent crack propagation. Transformation toughening of zirconia is the prominent mechanism for enhancing the fracture toughness of zirconia-reinforced composites [1]. In addition to this mechanism, crack deflection and crack bridging are also important to increase the fracture toughness of composite materials [2–11]. Metallic inclusions can limit the application of ceramic composites in high temperatures or aggressive environments, ceramic-ceramic composites on the other hand should be all-purpose composites.

In contrast, increasing the toughness of a material should not lead to a decrease in its strength. Traditional zirconia-alumina composites often represent this conflict between toughness and strength. Zirconia/alumina composites typically consist of a zirconia or alumina matrix and dispersed Al_2O_3 or ZrO_2. In the first case, the composite is named ATZ and in the second case, ZTA. In both cases, the fracture toughness of the ceramic matrix material increased. ZTA composites with 5 to 30 vol% concentration of zirconia inclusions have been studied very extensively over the last 20 years [9–17]. ATZ composites with the same concentration of alumina particles in zirconia ceramics have been studied less extensively [2, 18]. Interest in ATZ materials has heightened with the application of ATZ composites for dental and orthopaedic implants. The decrease in the content of inclusions in composite and nanocomposite materials was due to the fact that "the highest strength or fracture toughness is mostly achieved when only a few percent of the second-phase particles are dispersed in matrix material" [19]. Moreover, ceramics with a low percentage of second-phase particles exhibit better sinterability, while dispersed particles have a greater possibility of existing in matrix grains. All toughening mechanisms that are inherent to zirconia, such as transformation toughening, microcracking, deflection and bridging processes based on zirconia inclusions, were studied in order to explain the increase in the fracture toughness of ZTA and ATZ composites.

Over the past few years, new zirconia- and alumina-based composites have been developed and several authors have reported their improved mechanical properties compared to monolithic materials [4–6]. The correlation between the fracture toughness values, the content of inclusions and the structures of the composite materials was determined by Li [2], Shin *et al.* [9], Tuan and Chen [10, 11]. The fracture toughness changes caused by transformation toughness, crack deflection and crack bridging for

* Corresponding author: igord69@ukr.net

zirconia-alumina composites were calculated and compared with experimentally observed data. It was found that the indentation fracture toughness value increased to $1-2$ MPa·m$^{1/2}$ (nearly $15-20$ %) with an increase in the alumina amount in zirconia matrix of up to 20 % and more. In these studies, as well as in numerous other studies [13-18], different types of mixing were used for composite powder preparation. The Tosoh TZ-3Y-type zirconia powder with average primary particle size from 25 to 90 nm and Baikowski α-Al$_2$O$_3$ with average particle size from 0.25 to 1.6 µm were usually used as initial powders. But Tan and Yang [38] established the non-monotonic behaviour of the fracture toughness of alumina/SiC composites depending on the concentration of SiC particles in alumina matrix. At small SiC particles concentrations (8 %), fracture toughness doubles. Volume fractions of SiC particles higher or lower than this value reduce the toughening effect. The composite was fabricated by means of direct coagulation casting technology. The theoretical calculation for such composites was made by Levin [7]. "The model suggests that the increase in fracture toughness should be obtained only for small additions (less than 5 wt%) of SiC". The authors linked this effect with a change in the fracture mode observed in alumina on the addition of SiC particles. The analogical K_{1C} curve behaviour was found for ZrO$_2$-Ni nanocomposite while the K_{1C} for the microcomposite only decreases with the increase in Ni particle concentration [3].

In the case of zirconia-alumina system, a limited study started examination of other methods to obtain powders, for example ultrasonic, colloidal technique [4] and coating methods [16,32]. In our previous study [20] on 3Y-TZP-NiO composite, an increase in the indentation fracture toughness to $70-80$ % was determined in comparison with 3Y-TZP matrix material when the NiO concentration changed from 7 to 15 wt%. Therefore, the method used to prepare composite nanopowders plays a major role in the formation of the structure and properties of composite materials during sintering. In the case of zirconia-based nanocomposites, especially at low concentrations of alumina inclusions, investigations that have studied the correlation between the method of nanopowder preparation, nanocomposite structure and mechanical properties, are practically unknown.

In this study, we investigated the effect of nanopowder synthesis methods and alumina concentration on the structure and mechanical properties of 3Y-TZP/alumina ceramic composites.

II. Experimental Procedure

(1) Material and specimen preparation

ZrO$_2$-3 mol% Y$_2$O$_3$ nanopowders (3Y-TZP) and ZrO$_2$-3 mol% Y$_2$O$_3$ + n% Al$_2$O$_3$ were synthesized with a co-precipitation technique using ZrOCl$_2$·nH$_2$O, Y(NO$_3$)$_3$·nH$_2$O and AlCl$_3$·6H$_2$O salts. The amount of alumina was varied from 0.5 to 5 wt%. All chemicals used were of chemical purity (SiO$_2$ <0.008 wt%, Fe$_2$O$_3$ <0.01 wt%, Na$_2$O <0.01 wt%). The technological aspects of the precipitation process were described in [21,22]. After washing and filtration, the hydrogel was dried in a microwave furnace with an output power of 700 W and at a frequency of 2.45 GHz. The dried zirconium hydroxides and composites were calcined in a resistive furnace at 1000 °C with a dwelling time of 2 h in order to compare our results with data from the study by Li [2] and other data obtained with Tosoh powders with similar initial zirconia particle sizes. This variant was named CT.

For the control samples, an appropriate amount of commercially available α-Al$_2$O$_3$ powder was mixed with obtained 3Y-TZP nanopowders in distilled water. The α-Al$_2$O$_3$ particle size distribution was wide enough with an average size at 1 µm (manufacturer's data). This mixture was planetary-milled (MSK-SFM-1 MTI Corp., USA) at 400 rpm for 10 h using YSZ milling media. This variant was named BM.

Cylindrical (20 mm in diameter and 3 mm in height) and rectangular (45·4·4 mm) specimens were prepared firstly by means of uniaxial cold pressing, then isostatic pressing at 200 MPa and finally pressureless sintering at 1500 °C for 1 h.

(2) Microstructure, phase analysis and mechanical properties measurements

The powders and sintered specimens were characterized by means of XRD (Dron-3) with Cu-Kα radiation for crystallite sizes and quantitative phase analyses with a proven method [23]. Particle sizes of different calcined powders were estimated by means of transmission electron microscopy (TEM) (JEM 200, Jeol, Japan). Reliable data were obtained by analysing data from 30 TEM fields.

The flexural strength was measured using a four-point bending test on polished samples with a cross-head speed of 0.5 mm/min (Tinius Olsen H50kT, USA). The inner and outer spans were 20 and 40 mm, respectively. The measurements were conducted on $8-10$ samples for each variant of composition and method of powder preparation. The hardness and fracture toughness of the materials were measured at room temperature with the Vickers indentation technique (Vickers tester TP-7p-1) on mirror-polished surfaces with a 98 and 196 N load, respectively. At 196 N loads, the Palmqvist-type cracks were propagated in 3Y-TZP and composite with alumina. The fracture toughness values were calculated on the basis of the Nihara equation for Palmqvist-type cracks [24]. The measurements were conducted on three samples for each composition and method of preparation. On each sample, 20 indentations were made. The density was measured with the Archimedes method. The microstructures of the ceramics were studied by means of scanning electron microscopy (JSM 6490LV and JSM-7100F Jeol) after the surfaces and fracture surfaces had been polished.

III. Results and Discussion

(1) Powders and sintered composites characteristics

Transmission electron microscopy (TEM) results of nanopowders synthesized by co-precipitation and calcined at 1000 °C are shown in Fig. 1a, b. According to the TEM and X-ray diffraction (XRD) data, the average particle sizes of matrix 3Y-TZP nanopowder were 32 nm. Zirconia in the powders was represented by the tetragonal

phase (space group P42/nmc) (Fig. 2). The mean particle size of nanopowders obtained with the co-precipitation technique decreased from 32 to 19.3 nm with increasing concentrations of Al_2O_3 from 0 to 5 wt%, respectively. Incorporation of Al^{3+} cations into the ZrO_2 particles limited its crystallization [25] and consequently decreased the particle size of zirconia-alumina composite powders during calcination. The composite powder obtained by ball-milling 32 nm 3Y-TZP nanopowder with commercial α-Al_2O_3 powder is shown in Fig. 1c. After milling, the particle sizes of ZrO_2 did not change and the majority was smaller than 30 – 35 nm. The TEM investigation could not distinguish zirconia and crushed alumina particles smaller than 40 nm, so particles larger than 40 nm were α-Al_2O_3. The Al_2O_3 particle size distribution larger than 40 nm is represented in Fig. 1d. We can conclude that the average particle size of Al_2O_3 particles after milling process was estimated at 150 – 200 nm. This data correspond to data from other studies [13–18], where the TZ-3Y Tosoh powders were mixed with sub-micron size alumina powders.
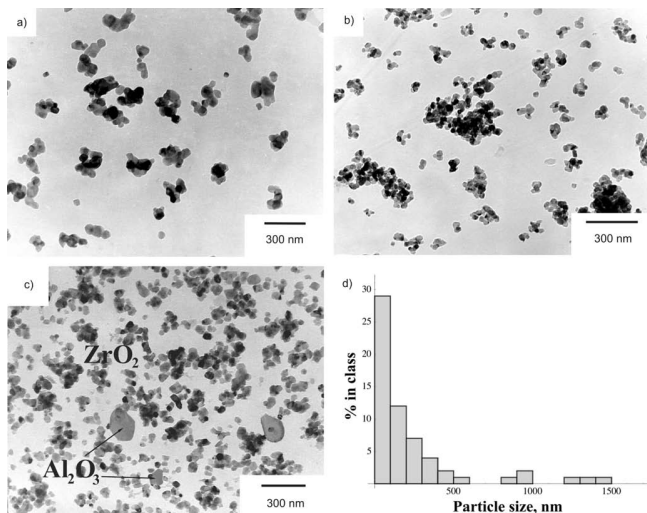

Fig. 1 : TEM structure of the 3Y-TZP-n Al_2O_3 nanopowders, obtained with the co-precipitation technique and calcined at 1000 °C: a – 0 wt% Al_2O_3, b – 2 wt% and c – by ball-milling 32 nm 3Y-TZP powder with α-Al_2O_3, d – α-Al_2O_3 particle size distribution in the BM composite after ball-milling.

According to XRD results, the phase composition of zirconia after sintering in composites and matrix materials did not change (Fig. 2). The phase composition was 9 – 11 % cubic phase and the rest tetragonal phase. Alumina in the sintered composites was represented by α-Al_2O_3. From XRD data (peak on 43,36°) we can identify the α-Al_2O_3 in the composite powder and sintered material that was obtained with the ball-milling technique (Fig. 2c). In contrast, in the nanocomposite powder obtained with the co-precipitation technique, the (101) α-Al_2O_3 reflex was not found during powder characterization but appears only in the sintered material (Fig. 2b). By means of SEM analysis, the macroscopic difference in alumina grain distribution in the composite structure was found after the use of a different powder preparation method (Fig. 3). This is a typical intercrystalline type of composite structure [25,26]. More uniform distribution of Al_2O_3 grains was determined in the composite structure obtained with the co-

precipitation technique (CT) in comparison with material obtained with the ball-milling (BM) technique. Higher magnification allows estimation of the average sizes of grains of tetragonal and cubic phases as well as the intercrystalline Al_2O_3 inclusions.
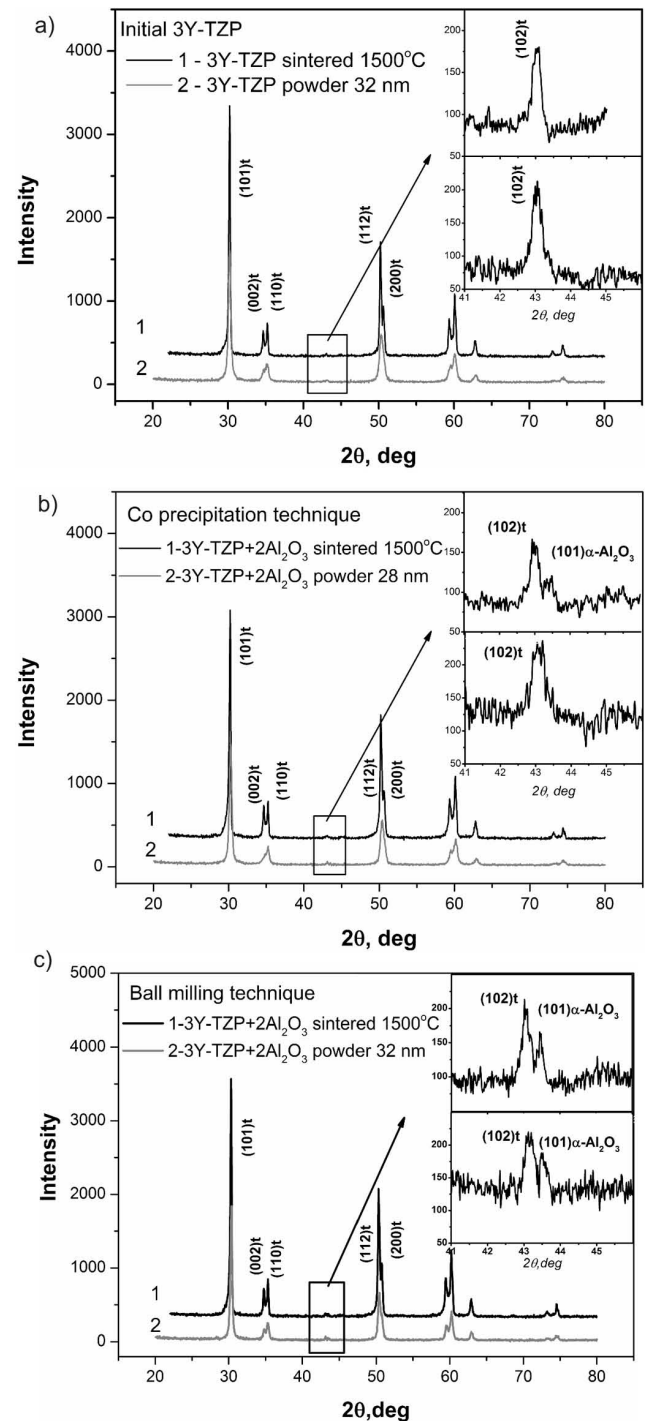

Fig. 2 : XRD data of 3Y-TZP and 3Y-TZP-2 wt% Al_2O_3 powder and ceramics. Initial 3Y-TZP – a), 3Y-TZP-2 wt% Al_2O_3 composite obtained with the co-precipitation technique – b) and ball-milling technique – c). In the inserts, the regions 40 – 45° are shown.

The average grains sizes with tetragonal and cubic phases were 0.2 – 0.4 μm and 2 – 3 μm, respectively. These values practically did not change depending on alumina content and powder preparation method. Moreover, the phase composition of zirconia (10 – 12 % C-phase and 88 – 90 % T-phase) did not depend on the powder prepara-

tion method either. These structure parameters are typical for such chemical composition and sintering conditions. With SEM analysis, it was identified that the average size of intercrystalline Al_2O_3 grains in the CT composite as 0.4 μm and maximal grain size – 1.1 μm. For the BM composite, estimation of average and maximal grain size is very difficult because the alumina inclusions are extremely agglomerated. The inclusion size distribution is wide, and the average size of individual inclusions in BM composite can be estimated as 0.5 – 1 μm and size of aggregated inclusions reaches 2 – 3 microns. At a concentration of 5 wt%, the agglomeration of inclusions in the CT composite had only started and in composites with 1 and 2 wt% Al_2O_3 intercrystalline alumina inclusions are represented by individual grains.

(2) Mechanical properties (density, strength, hardness, and indentation fracture toughness)

All samples, except for the composite with 5 wt% Al_2O_3, were sintered to greater than 99 % theoretical density. Determination of the crack length under Vickers indentation and evaluation of indentation fracture toughness for these samples is possible and approved in other studies [2, 4, 8, 13 – 16]. Excessive porosity in the 5 wt% Al_2O_3 sample may show a shortened crack length and increased K_{1C} value [2, 24, 27].

All mechanical properties of the sintered composites are shown in Table 1. It should be noted that the four-point bending strength values decreased only on 10 % from 850 ± 60 MPa to 760 ± 70 MPa with increasing Al_2O_3 amounts from 0 to 5 wt% for the CT composite and to 780 ± 90 MPa for the BM composite. Hardness values for both types of composites changed slightly: from 12.6 ± 0.2 GPa to 12.45 ± 0.3 GPa for the co-precipitation technique and from 12.6 ± 0.2 GPa to 13.1 ± 0.3 GPa for the ball-milling technique, with increasing Al_2O_3 amounts from 0 to 5 wt%.

Analysis of crack propagation after Vickers indentation showed that the crack length in the matrix 3Y-YZP material was 374 μm (Fig. 4a). The crack length in the CT composite materials decreased to 210 μm at 1 wt% concentrations of Al_2O_3. At concentrations of 2 and 5 wt%, the crack length stabilized at a level of 220 – 230 μm (Fig. 4b).

In the case of the BM composites with 1, 2 and 5 wt% Al_2O_3, the crack length was 345, 330 and 320 μm, respectively (Fig. 4c). Because the density of the BM samples did not change, the monotonic decrease in crack length for the BM composites could be linked with the increase in alumina content. This result is confirmed by theoretical calculations from studies [2, 28]. For the CT composites, such a non-monotonic decrease in crack length could not be explained based on simple dependences.
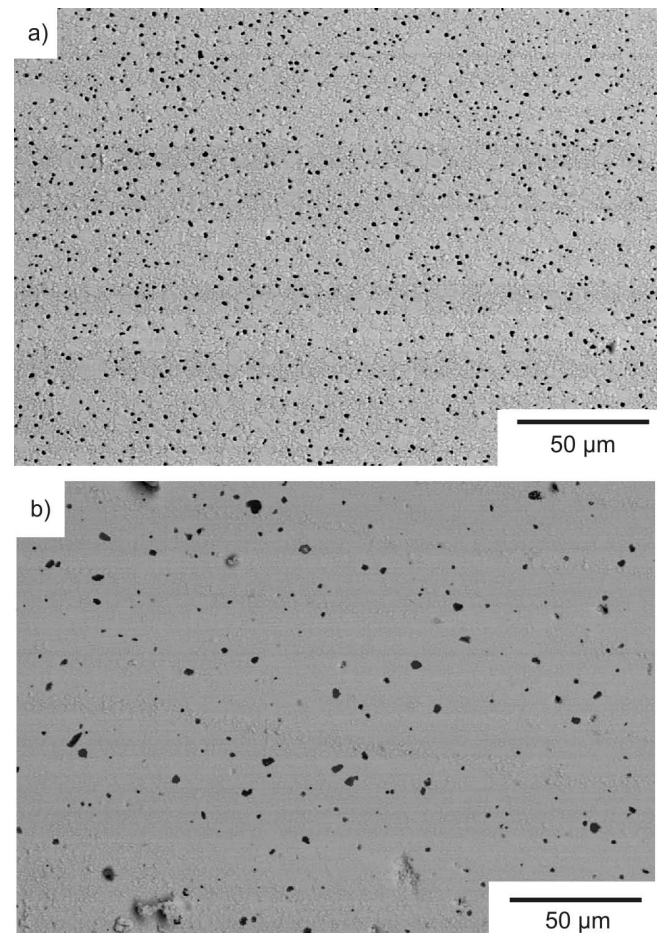
Fig. 3 : SEM microstructure of 3Y-TZP-2 wt% Al_2O_3 composite ceramic materials obtained by means of sintering co-precipitated powders – a) and ball-milled powders – b).

Table 1: Mechanical properties of sintered composites

| Composition	Method of preparation	Hardness, GPa	Fracture toughness, MPa·m$^{1/2}$	Bending strength, MPa	Density, g/cm^3
3Y-TZP	Coprecipitation	12.6±0.2	5.8±0.4	850±60	6.07±0.01
3Y-TZP+0.5 wt%Al_2O_3	Coprecipitation	12,5±0.2	7.6±0.4	820±54	6.05±0.01
3Y-TZP+1 wt%Al_2O_3	Coprecipitation	12.4±0.3	11.2±0.6	770±40	6.01±0.01
3Y-TZP+2 wt%Al_2O_3	Coprecipitation	11,9±0.2	10.4±0.6	805±60	5.99±0.02
3Y-TZP+5 wt%Al_2O_3	Coprecipitation	12.45±0.3	9.4±0.8	760±70	5.87±0.02
3Y-TZP+1 wt%Al_2O_3	Ball-milling	12.9±0.2	6.1±0.3	840±56	6.03±0.01
3Y-TZP+2 wt%Al_2O_3	Ball-milling	12.97±0.2	6.4±0.4	807±51	6.00±0.02
3Y-TZP+5 wt%Al_2O_3	Ball-milling	13.1±0.3	6.7±0.6	780±90	6.01±0.01
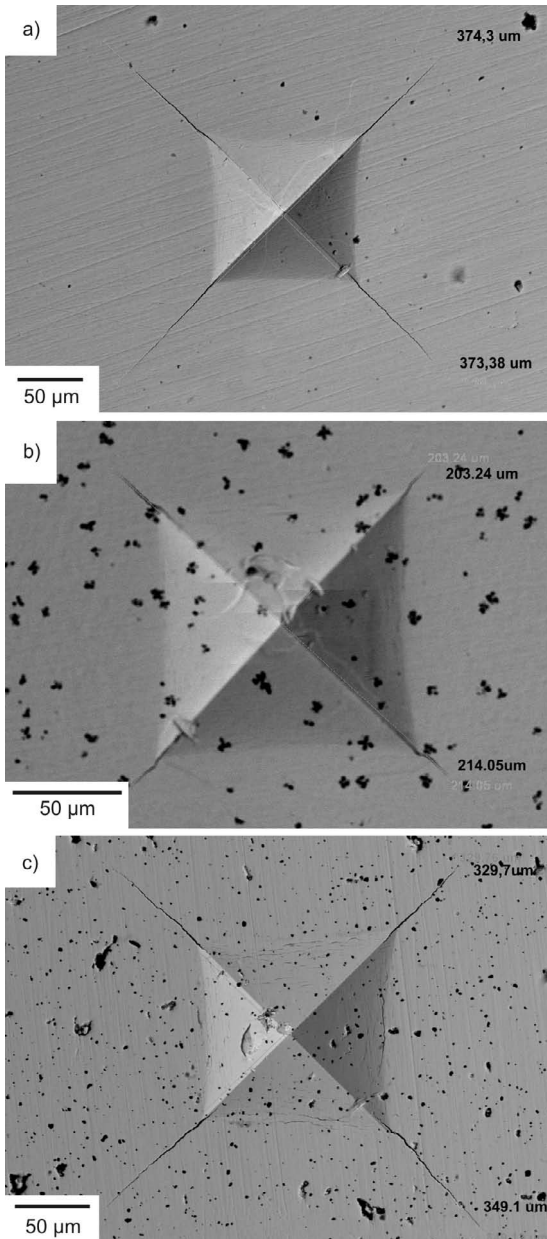
Fig. 4 : SEM images of Vickers indentation (196 N) and cracks at the surface of sintered composite samples obtained from co-precipitated (a, b) nanopowders and ball-milled (c) powders: a – matrix 3Y-TZP, b, c – 3Y-TZP+2 wt% Al_2O_3.
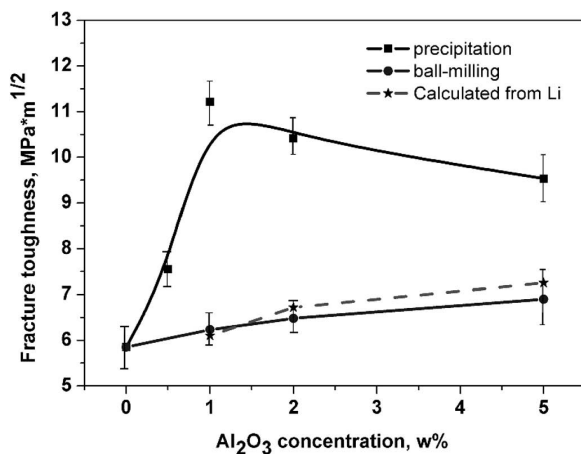

Fig. 5 : Dependence of indentation fracture toughness of 3Y-TZP-Al_2O_3 composite sintered at 1500 °C on Al_2O_3 content for two methods of composite powder preparation.

Thus, with identical chemical compositions, sintering conditions, and measuring methods, the crack propagation depended on the powder preparation method and the process of composite structure formation. For continuity with previous studies, we will use the K_{1C} calculation equations from [2]. We know that the absolute toughness values obtained by the indentation method could be overestimated, but this technique has been approved by many authors to provide an estimation of the fracture toughness values.

Fig. 6 shows the change in the indentation fracture toughness value for 3Y-TZP-Al_2O_3 composites as a function of the alumina concentration. The results showed that the Al_2O_3 inclusions increased the indentation fracture toughness of 3Y-TZP ceramics. K1C of the 3Y-TZP-Al_2O_3 composite depended on the method used to prepare the composite powder.
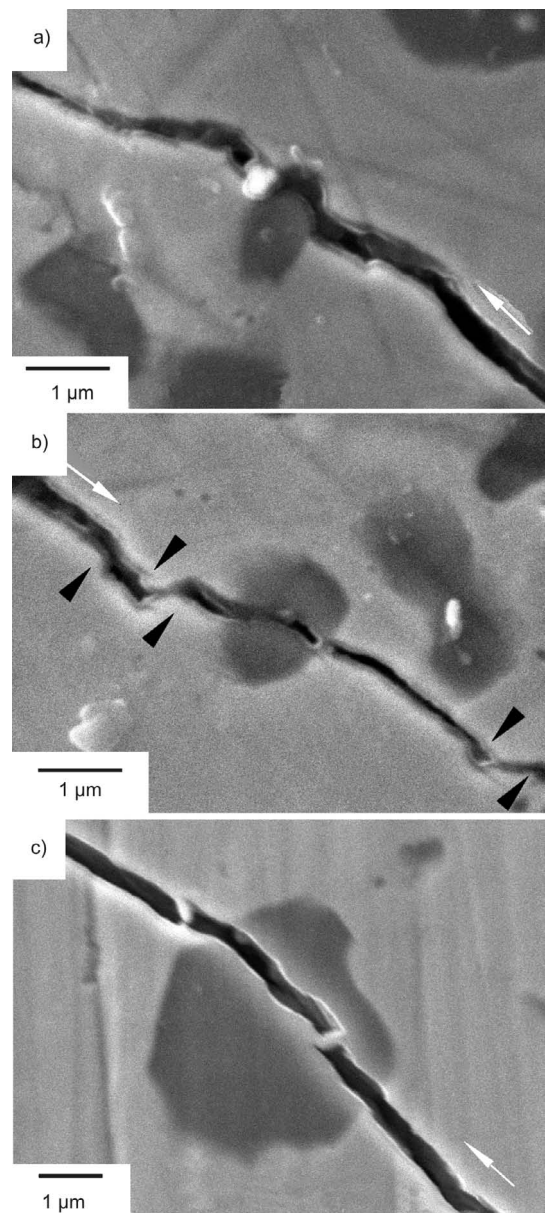

Fig. 6 : Crack propagation in 3Y-TZP- Al_2O_3 composites obtained from co-precipitated nanopowders (a, b) and from ball-milled powders (c). The dark grains are Al_2O_3. Directions of crack propagation are marked with a white arrow. The black arrows show the high level of crack deviation..

Table 2: Monoclinic fraction in polished and fractured surfaces of sintered composite samples.

Composition	Preparation method	Amount of M-phase,%	
		polished surface	fractured surface
3Y-TZP	Coprecipitation	0; 2; 0	34.0; 28.7; 36.0
3Y-TZP+0.5 wt% Al_2O_3	Coprecipitation	1; 2; 0	35.0; 37.3; 31.7
3Y-TZP+1 wt% Al_2O_3	Coprecipitation	2; 1; 0	34.5; 32.0
3Y-TZP+2 wt% Al_2O_3	Coprecipitation	0; 3; 1	35.3; 31.4
3Y-TZP+1 wt% Al_2O_3	Ball-milling	1; 0; 2	32.7; 29.6; 28.3
3Y-TZP+2 wt% Al_2O_3	Ball-milling	0; 0; 2	26.4; 34.5

Since the concentrations of alumina in the composite were small and identical for the CT and BM samples, we believed that the behaviour of crack propagation was not due to the influence of the alumina additions on transformation toughening mechanism, as described by Li and Evans in [2, 27]. But for verification of this position, we, by analogy with Kern's results [16], analysed the M-phase fraction on polished and fractured surfaces of the initial 3Y-TZP and both composite samples. As mention above, the amount of M-phase on polished surfaces of all samples was less than 2 %. The amounts of M-phase on the fractured surfaces of 3Y-TZP and both composite samples are shown in Table 2. It should be noted that we are unable to perform XRD of the fractured surfaces of all samples, because part of fractured surfaces was curved. In Table 2 we have presented the M-phase data for all samples that could be measured.

As you can see from Table 2, the amount of M-phase did not depend on the alumina amount and powder preparation method. The amount of M-phase in the initial 3Y-TZP and composite ceramics is equal at ~30 % and transformability, which is defined as the difference in monoclinic percentage in fractured and polished surfaces, in these samples is equal. Consequently, the mechanical properties of zirconia in the initial sample and in the composite ceramics are conditioned by transformation toughening from the T-M phase transition too, but the minute amount of alumina and method of sample preparation did not affect the K_{1C} values. In addition, if we analysed the level of residual stresses and its contribution on reinforcement mechanisms with the Li [2] or Kern [16] equation, we obtained the equivalent results for BM and CT materials.

$$\Delta K = 2q(2(\lambda - d)\pi)^2 \quad (1),$$

where *q* is the thermal residual stress in matrix, λ is the average interparticle spacing, which can be related to the average diameter *d*, and the volume fraction, *f*, of particles as follows:

$$\lambda = 1.085 d/f^{0.5} \quad (2),$$

and *q* can be calculated with the following equations [2]:

$$q = -2f\beta\Delta\alpha E_m/A \quad (3),$$

where β and *A* are the composition from the Young and Poisson moduli of ZrO_2 and Al_2O_3. But in these equations all data are the same: Young and Poisson moduli and thermal expansion coefficients for ZrO_2 and Al_2O_3, vol-

ume fraction of the alumina and the average grain size of the alumina grains. Based on Li, Kern, Awaji and other calculations based on Timoshenko and Gudier theory, we know that the second-phase (Al_2O_3) particles are under hydrostatic compressive pressure and under tensile tangential stress. These facts did not explain the difference in K_{1C} for composite materials obtained with different techniques.

In this case, the crack deflection and crack-bridging process as a result of the alumina inclusions should be different depending on the method used, because different methods lead to the formation of different structures. Both effects were observed during our experiments (Fig. 6). The values of toughening increment based on crack deflection toughening in 3Y-TZP-Al_2O_3 composites were estimated by comparison to a study by Li [2] according to the Faber, Evans [28] and Taya [29] models. The total calculated value of toughness increase for the deflection mechanism was $0.05 - 0.2$ MPa·m$^{1/2}$ for 0.5 and 5 wt% Al_2O_3, respectively. The toughening increment resulting from grain bridging [30] for an average Al_2O_3 grain size of 1 µm was $0.03 - 0.3$ MPa·m$^{1/2}$ for 0.5 and 5 wt% Al_2O_3, respectively. For composites obtained from ball-milled powders, the effect of crack bridging should be more significant owing to the larger grain size of the inclusions (Fig. 6c) [2, 17, 28]. For composites obtained by means of ball milling, the increase in the K_{1C} value as a function of alumina content can be explained by the superposition of bridging and deflection processes accompanied with residual stresses, as shown by Li [2] and confirmed by calculations for an average alumina inclusion size of 1 µm. However, using the superposition of these two mechanisms, we cannot explain the differences between experimental and calculated K_{1C} increment data for composites obtained using the co-precipitation technique. As is known, the deflection and bridging processes strongly depend on composite structure, but we cannot find any significant differences in macroscopic composite structures.

IV. Discussion

The crack deflection process (Fig. 6a) is well-known for zirconia-toughened alumina systems, but the simple physical principle written by Yeomans [33] makes the process shown in Fig. 6b nearly impossible owing to the Young's modulus of Al_2O_3 inclusion (370 – 390 GPa), that is approximately two times higher than in a zirconia matrix

(198 – 205 GPa). But in our experiments the crack passes through the alumina inclusions. But what object should deflect the crack in the direction of the alumina grain? The Levin [7] calculations for Al_2O_3-SiC composites predict that the local compressive microstresses due to adjacent SiC particles are required on alumina grain boundaries in order to deflect the crack into the grain. But for the CT and BM composites, we found crack deflection into Al_2O_3 grains in both cases.
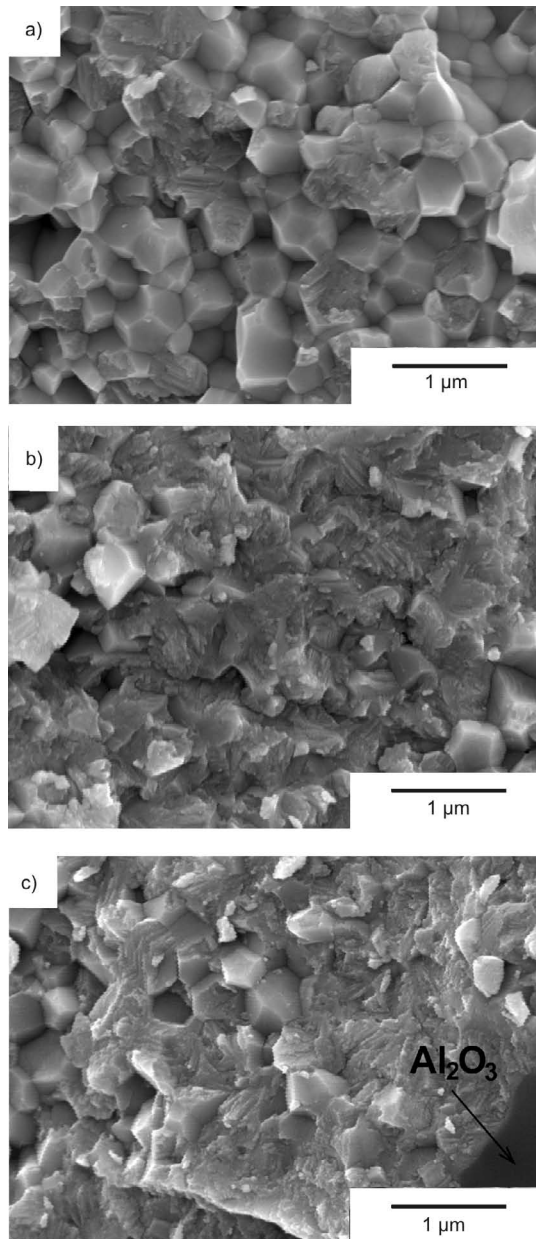

Fig. 7: SEM images show the increase in the part of transcrystalline fracture in 3Y-TZP- Al_2O_3 composites – b, c) in comparison with matrix 3Y-TZP material – a). Structure of CT composite – b) and BM composite – c).

The higher value of fracture toughness of the CT composite is explained by the increase in number of crack deviations as well as deflection angles (Fig. 6b). In the matrix material and BM composite (Fig. 4 a, c), the measured crack length was longer than that in the CT composite (Fig. 4b), suggesting an improvement in fracture toughness. It is also observed by means of TEM and SEM that

in the CT and BM composites, the part of transcrystalline fracture (Fig. 7) is higher than that in the matrix material where the intercrystalline fracture mode was predominant. It suggests that the small alumina addition increased the zirconia-zirconia interparticle interaction during sintering by intensification of volume diffusion mechanism as shown by Matsui [34] and in many others works [34–38]. It should be noted that the analogical non-monotonic behaviour dependence of the fracture toughness value on the inclusion concentration was studied in [38] for Al_2O_3-SiC nanocomposites. This effect is conditioned with fluctuating residual stresses generated by nanoparticles within the matrix grains that deflect the transgranular cracking path, creating additional fracture surface. The analogical structure changes from intercrystalline to transcrystalline character of fracture surface also were found for all cases of nanocomposites studied in [2, 16, 34–38], but the inclusions concentration in these studies was high enough (more than 5 %). Consequently, the dispersed inclusions increase the part of transgranular fracture, crack deviation and fracture toughness. And the crack deflection process in the CT composite was more effective in comparison with that in the BM composite.

Thus, the microscopic difference in composite structure, particularly in zirconia grains, may explain the increasing role of the deflection process for the CT composite in comparison with the matrix material and BM composite.

We suggest that two distinctive features are responsible for the fracture toughness difference in CT and BM composites: difference in the distribution of Al^{3+} ions during the powder preparation processes, and formation of different types of Al_2O_3 inclusions during sintering when we used the two different staring powders.

When the method of co-precipitation is used, Al^{3+} ion distribution in the starting composite nanopowder is more uniform compared to that with the mechanical mixing technique. Al^{3+} solubility in zirconia is very low (0.1 % at 1300 °C [34]), and during sintering the active diffusion of ions Al^{3+} from the volume to the grain boundary or triple junctions takes place. The size of alumina inclusions increased from 50 nm to several microns on an increase in temperature from 1300 to 1500 °C. Consequently, the random alumina distribution transforms to a discrete distribution and the alumina intercrystalline grains are formed.

But Matsui *et al.* [35, 36] showed that Al^{3+} ions segregate along grain boundaries in both T-T and C-T zirconia grains over a width of 5–10 nm at an initial Al_2O_3 concentration of 0.2 wt%. In our experiments, the EDS analysis in places without visible Al_2O_3 inclusion showed the 0.2–0.4 wt% Al_2O_3. The process of grain growth and sintering is competing with Al^{3+} segregation and redistribution during heating of co-precipitated nanopowders. Some inclusions can be captured by growing grains and turn into intratype inclusions [37]. An amount of alumina can remain on sub-grains and grains boundaries. The complex structure (Fig. 8) could be formed during sintering of co-precipitated nanopowders. The final structure consists of matrix grains and sub-grains with or without alumina segregations [35, 36], inter- and intratypes of inclusions [37]. The crack propagation from such a structure should be hampered.
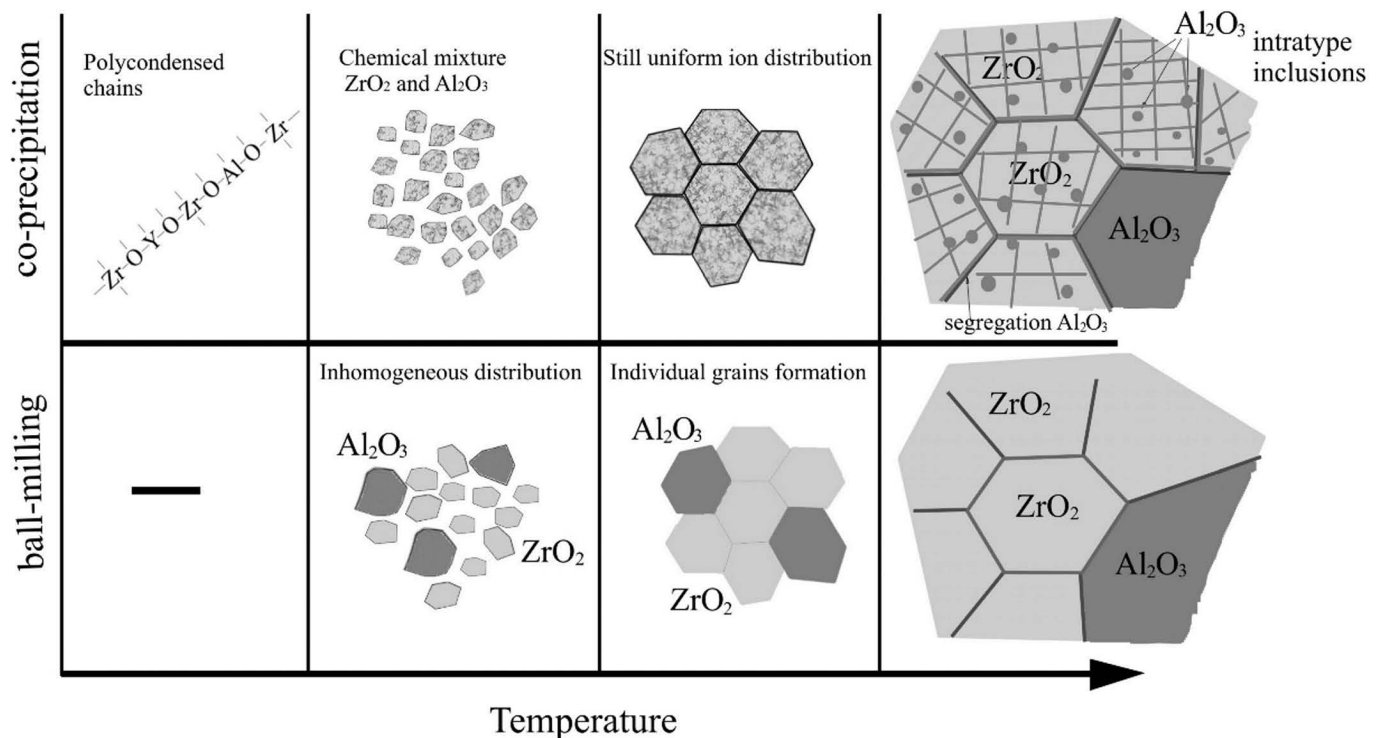
Fig. 8: Scheme of composite structure formation for the different methods of powder preparation.

The influence of intratype inclusions on fracture toughness of composites was discussed by Tan and Yang [37]. "Typically, the main crack extends intergranularly along the grain boundary since the fracture resistance of the grain boundary is lower than that of the grain lattice. The strong cohesion between the nano-particle and the matrix enables the crack to make a turn within the nano-particle and to enter the matrix grain." This process led to increases in the transgranular fracture of matrix grains as shown in Fig. 8b and to maximize the mode I of the stress intensity factor for CT composites.

In the case of ball-milling powder preparation method, the Al_2O_3 particles located only on zirconia grain surfaces and intragranular alumina inclusions in zirconia grains during sintering could not be formed in appropriate amount, because the solubility of Al^{3+} ions in zirconia is too low. Consequently, an increase in the K_{1C} value through the intratype inclusions in BM composite is absent.

Thus, the increase in the K_{1C} value of zirconia ceramics with a small amount of alumina sintered from nanopowders obtained using co-precipitation techniques can be conditioned through a series of processes for composite structure formation during precipitation, crystallization, and sintering of nanopowders. These processes differ strongly from structure formation processes in composites produced from ball-milled powders.

The formation of complex multilevel composite structures, such as Al^{3+} ion segregation on zirconia grain boundaries and intracrystalline alumina inclusions in zirconia grains, have increased the amount of object that has taken part in crack deflection processes, and the virtual value of inclusion concentration in equation should be increased. The lack of such structure abnormalities in composite structures sintered from ball-milled powders led to a slight increase in the K_{1C} value due to the geometric effect of the inclusions in the composite structure.

V. Conclusions

Based on a study of the indentation fracture toughness of 3Y-TZP-Al_2O_3 micro- and nanocomposites, the following conclusions can be made:

– it was found that the indentation fracture toughness of 3Y-TZP-Al_2O_3 composites depends on the method of powder preparation;

– the use of co-precipitated nanopowders enables an increase in the fracture toughness value while the strength value does not change;

– an increase in the K_{1C} value of zirconia ceramics with a small amount of alumina, sintered from nanopowders obtained using co-precipitation techniques, can be conditioned through a series of processes for composite structure formation during precipitation, crystallization, and sintering of nanopowders;

– multi-level system of Al_2O_3 inclusions in combination with the enrichment of zirconia grain boundaries enables realization of a new level of crack inhibition mechanisms and increases the fracture toughness of zirconia ceramics.

References

1 Hannik, R., Kelly, P., Muddle, B.: Transformation toughening in zirconia-containing ceramics, *J. Am. Ceram. Soc.*, **83**, [3], 461 – 87, (2000).

2 Li, J., Watanabe, R.: Fracture toughness of Al_2O_3-particle-dispersed Y_2O_3 partially stabilized zirconia, *J. Am. Ceram. Soc.*, **78**, [4], 1079 – 1082, (1995).

3 Lopez-Esteban, S., Rodriguez-Suarez, T., Esteban-Betego, F., Pecharroma, C., Moya, J.: Mechanical properties and interfaces of zirconia/nickel in micro-and nanocomposites, *J. Mater. Sci.*, **41**, [16], 5194 – 5199, (2006).

4 Vasylkiv, O., Sakka, Y., Skorokhod, V.: Low-temperature processing and mechanical properties of zirconia and Zirconia-Alumina nanoceramics, *J. Am. Ceram. Soc.*, **86**, [2], 299 – 304, (2003).

5 Kern, F.: Ytterbia-neodymia-costabilized TZP – breaking the limits of strength -toughness correlations for zirconia?, *J. Eur. Ceram. Soc.*, **33**, [5], 965 – 973, (2013).

6 Bartolome, J.F., Gutierrez-Gonzalez, C.F., Torrecillas, R.: Mechanical properties of alumina-zirconia-Nb micro-nanohybrid composites, *Comp. Sci. and Tech.*, **68**, [6], 1392 – 1398, (2008).

7 Levin, I., Kaplan, W., Brandon, D., Layyous, A.: Effect of SiC submicrometer particle size and content on fracture toughness of alumina-SiC "nanocomposites", *J. Am. Ceram. Soc.*, **78**, [1], 254 – 256, (1995).

8 Szutkowska, M.: Fracture resistance behavior of alumina-zirconia composites, *J. Mater. Process Tech.*, **153 – 154**, 868 – 874, (2004).

9 Shin, Y., Rhee, Y., Kang, S., Experimental Evaluation of Toughening Mechanisms in Alumina-Zirconia Composites, *J. Am. Ceram. Soc.*, **82**, [5], 1229 – 1232, (1999).

10 Chen, R.Z., Tuan, W.H.: Toughening alumina with silver and zirconia inclusions, *J. Eur. Ceram. Soc.*, **21**, [16], 2887 – 2893, (2001).

11 Tuan, W.H., Chen, R.Z.: Interactions between toughening mechanisms: transformation toughening versus plastic deformation, *J. Mater. Res.*, **17**, [11], 2921 – 2928, (2002).

12 Lange, F.: Transformation toughening, *J. Mater. Sci.*, **17**, [1], 225 – 263, (1982).

13 Nevarez-Rascon, A., Aguilar-Elguezabal, A., Orrantia, E., Bocanegra-Bernal, M.H.: Compressive strength, hardness and fracture toughness of Al_2O_3 whiskers reinforced ZTA and ATZ nanocomposites: weibull analysis, *Int. J. Refract. Met. H.*, **29**, [3], 333 – 340, (2011).

14 Santos, C., Teixeira, L., Daguano, J., Rogero, S., Strecker, K., Elias, C.: Mechanical properties and cytotoxity of 3Y-TZP bioceramics reinforced with Al_2O_3 particles, *Ceram. Int.*, **35**, [2], 709 – 718, (2009).

15 Li, S., Izui, H., Okano, M., Zhang, W., Watanabe, T.: Microstructure and mechanical properties of ZrO_2 (Y_2O_3)-Al_2O_3 nanocomposites prepared by spark plasma sintering, *Particuology.* **10**, [3], 345 – 351, (2012).

16 Kern, F., Palmero, P.: Microstructure and mechanical properties of alumina 5 vol% zirconia nanocomposites prepared by powder coating and powder mixing routes, *Ceram. Int.*, **39**, [1], 673 – 682, (2013).

17 Kageyama, K., Harada, Y., Kato, H.: Preparation and mechanical properties of Alumina-Zirconia composites with agglomerated structures using pre-sintered powder, *Mater. Trans.*, **44**, [8], 1571 – 1576, (2003).

18 Nevarez-Rascon, A., Aguilar-Elguezabal, A., Orrantia, E., Bocanegra-Bernal, M.H.: On the wide range of mechanical properties of ZTA and ATZ based dental ceramic composites by varying the Al_2O_3 and ZrO_2 content, *Int. J. Refract. Met. H.*, **27**, 962 – 970, (2009).

19 Choi, S., Awaji, H.: Nanocomposites – a new material design concept, *Sci. Technol. Adv. Mat.*, **6**, 2 – 10, (2005).

20 Danilenko, I., Glazunov, F., Konstantinova, T., Volkova, G., Burkhovetski, V.: Effect of oxide nanofillers on fabrication, structure, and properties of zirconia-based composites, *J. Eur. Ceram. Soc.*, **33**, [12], 2321 – 2325, (2013).

21 Pilipenko, N., Konstantinova, T., Tokiy, V., Danilenko, I., Saakjants, V., Primisler, V.: Peculiarities of zirconium hydroxide microwave drying process, *Functional Materials*, **9**, [3], 323 – 327, (2002).

22 Konstantinova, T., Danilenko, I., Glazunova, V., Volkova, G., Gorban, O.: Mesoscopic phenomena in oxide nanoparticles systems: processes of growth, *J. Nanopart. Res.*, **13**, [9], 4015 – 4023, (2011).

23 Garvie, R.C., Nicholson, P.S.: Phase analysis in zirconia systems, *J. Am. Ceram. Soc.*, **55**, [6], 303 – 305, (1972).

24 Niihara, K.: A fracture mechanics analysis of indentation-induced palmqvist crack in ceramics, *J. Mater. Sci. Lett.*, **2**, [5], 221 – 223, (1983).

25 Navarro, L.M., Recio, P., Duran, P.: Preparation and properties evaluation of zirconia-based/Al_2O_3 composites as electrolytes for solid oxide fuel cell systems, *J. Mater. Sci.*, **30**, [8], 193l – 1938, (1995).

26 Bhaduri, S., Bhaduri, S.B.: Recent developments in ceramic nanocomposites, *J. Mater.* **50**, [1], 44 – 51, (1998).

27 Evans, A.G., Cannon, R.M.: Toughening of brittle solids by martensitic transformation, *Acta Metall. Mater.*, **34**, [5], 761 – 800, (1986).

28 Faber, K.T., Evans, A.G.: Crack deflection processes-I. theory, *Acta Metall. Mater.*, **31**, [4], 165 – 176, (1983).

29 Taya, M., Hayashi, S., Kobayashi, A.S., Yoon, H.S.: Toughening of a particulate-reinforced ceramic-matrix composite by thermal residual stress, *J. Am. Ceram. Soc.*, **73**, [5], 1382 – 1391, (1990).

30 Evans, A.G.: Perspective on the development of high-toughness ceramics, *J. Am. Ceram. Soc.*, **73**, [2], 187 – 205, (1990).

31 Naglieri, V., Palmero, P., Montanaro, L., Chevalier, J.: Elaboration of alumina-zirconia Composites: role of the zirconia content on the microstructure and mechanical properties, *Materials*, **6**, [5], 2090 – 2102, (2013).

32 Sommer, F., Landfried, R., Kern, F., Gadow, R.: Mechanical properties of zirconia toughened alumina with 10 – 24 vol% 1Y-TZP reinforcement, *J. Eur. Ceram. Soc.*, **32**, [15], 4177 – 4184, (2012).

33 Yeomans, J.A., Ductile particle ceramic matrix composites — Scientific curiosities or engineering materials?, *J. Eur. Ceram. Soc.*, **28**, [7], 1543 – 1550, (2008).

34 Matsui, K., Ohmichi, N., Ohgai, M., Enomoto, N., Hojo, J.: Sintering kinetics at constant rates of Heating: effect of Al_2O_3 on the initial sintering stage of fine zirconia powder, *J. Am. Ceram. Soc.*, **88**, [12], 3346 – 3352, (2005).

35 Guo, X., Yuan, R.: Roles of alumina in zirconia-based solid electrolyte, *J. Mater. Sci.*, **30**, [4], 923 – 931, (1995).

36 Matsui, K., Ohmichi, N., Ohgai, M., Yoshida, H., Ikuhara, Y.: Effect of alumina-doping on grain boundary segregation-induced phase transformation in yttria-stabilized tetragonal zirconia polycrystal, *J. Mater. Res.*, **21**, [9], 2278 – 2289, (2006).

37 Matsui, K., Yoshida, H., Ikuhara, Y.: Phase-transformation and grain-growth kinetics in yttria-stabilized tetragonal zirconia polycrystal doped with a small amount of alumina, *J. Eur. Ceram. Soc.*, **30**, [7], 1679 – 1690, (2010).

38 Tan, H., Yang, W.: Toughening mechanisms of nanocomposite ceramics, *Mech. Mater.*, **30**, [2], 111 – 123, (1998).